Electrical Engineering
https://doi.org/10.1007/s00202-025-03129-0

ORIGINAL PAPER

Segmented rotor: a viable alternative to flux-barrier design for small-diameter synchronous reluctance machines

M. A. H. Rasid[1] · Alejandro Ospina[2] · Vincent Lanfranchi[2] · Vladimir Kuptsov[3]

Received: 14 January 2025 / Accepted: 16 April 2025

Abstract
The flux-barrier rotor topology, widely recognized as optimal for synchronous reluctance machines (SynRM), has well-established design parametrization guidelines. However, these conventional design rules face challenges when applied to small-diameter applications, particularly where manufacturing constraints limit design options. This study investigates the applicability of conventional flux-barrier design principles in a SynRM with a 25.24-mm rotor diameter and evaluates alternative rotor configurations. A comparative analysis was conducted between two conventionally parameterized flux-barrier designs, an innovative segmented rotor topology, and a theoretical three-barrier design. Finite element analysis revealed that the segmented rotor achieves superior performance with a saliency ratio of 2.07 and torque density of 2.2×10^{-5} N·m/mm^3, comparable to larger machines reported in recent literature. At 5000 r/min and 50A, this configuration delivers 0.78 N·m torque with 45.75% efficiency and 0.63 power factor. Mechanical analysis confirmed structural integrity under high-speed operation, with maximum stress and deformation values of 6.2×10^5 N/mm^2 and 5.47×10^{-5} mm respectively. Experimental validation of a prototype largely corroborated simulation results though revealed higher torque ripple attributed to the modular stator construction necessitated by the small diameter. This study demonstrates that conventional flux-barrier design rules become less effective at small scales and presents a segmented rotor topology as a viable alternative, offering comparable performance while simplifying manufacturing processes.

Keywords SynRM · Saliency ratio · Flux barrier · Segmented rotor · Modular rotor

1 Introduction

Synchronous reluctance machine (SynRM) has been studied and optimized since 1990s and has found a place in the market via several manufacturers such as ABB, WEG, and Nidec. Pioneering research and development contributions by Lipo, Miller, Bianchi, and Pellegrino [1–4] have significantly advanced the field. Their work demonstrated that rotor designs featuring flux barriers aligned with the natural flux paths yield superior performance, offering enhanced torque density, improved saliency ratio, and improved power factor and efficiency.

In a SynRM without permanent magnet assistance, the machine is thermally and mechanically as robust as the squirrel-cage induction machine and it can even be combined with rotor bars to have the ability to line-start [5]. A design that prioritizes the torque produced will look to increase the difference between the direct and quadrature inductance ($L_d - L_q$) as shown in Eq. (1). With the inductance difference, the saliency ratio.

$\xi = L_d/L_q$ also needs attention as it is related to the power factor as can be approximated by Eq. (2).

$$T = \frac{3}{4} p\left(L_d - L_q\right) I_s^2 \sin 2\beta \tag{1}$$

$$cos\varphi = \frac{\frac{L_d}{L_q} - 1}{\frac{L_d}{L_q} + 1} \tag{2}$$

Figure 1 illustrates various flux barrier designs imple-

✉ M. A. H. Rasid
mahizami@ump.edu.my

1 Faculty of Manufacturing & Mechatronics Engineering Technology, Universiti Malaysia Pahang Al-Sultan Abdullah, 26600 Pekan, Malaysia

2 Roberval Laboratory, Université de Technology de Compiègne, 60203 Compiègne, France

3 MotorXP LLC US, 14271 Fern Avenue, Chino, CA 91710, USA

Published online: 14 May 2025

Table 4 Parameters to be optimized

Rotor	Param	Minimum	Maximum	Intervals in DOE	Units	Total simulation
FB1	ϑ_{b1}	22	40	2.5	[°]	8
FB2	ϑ_{b1}	23	33	2.5	[°]	5
Segmented	d_{seg}	3.0	7.2	0.6	mm	108 (8*12)
	g_{rot}	0.5	7.0	0.6	mm	

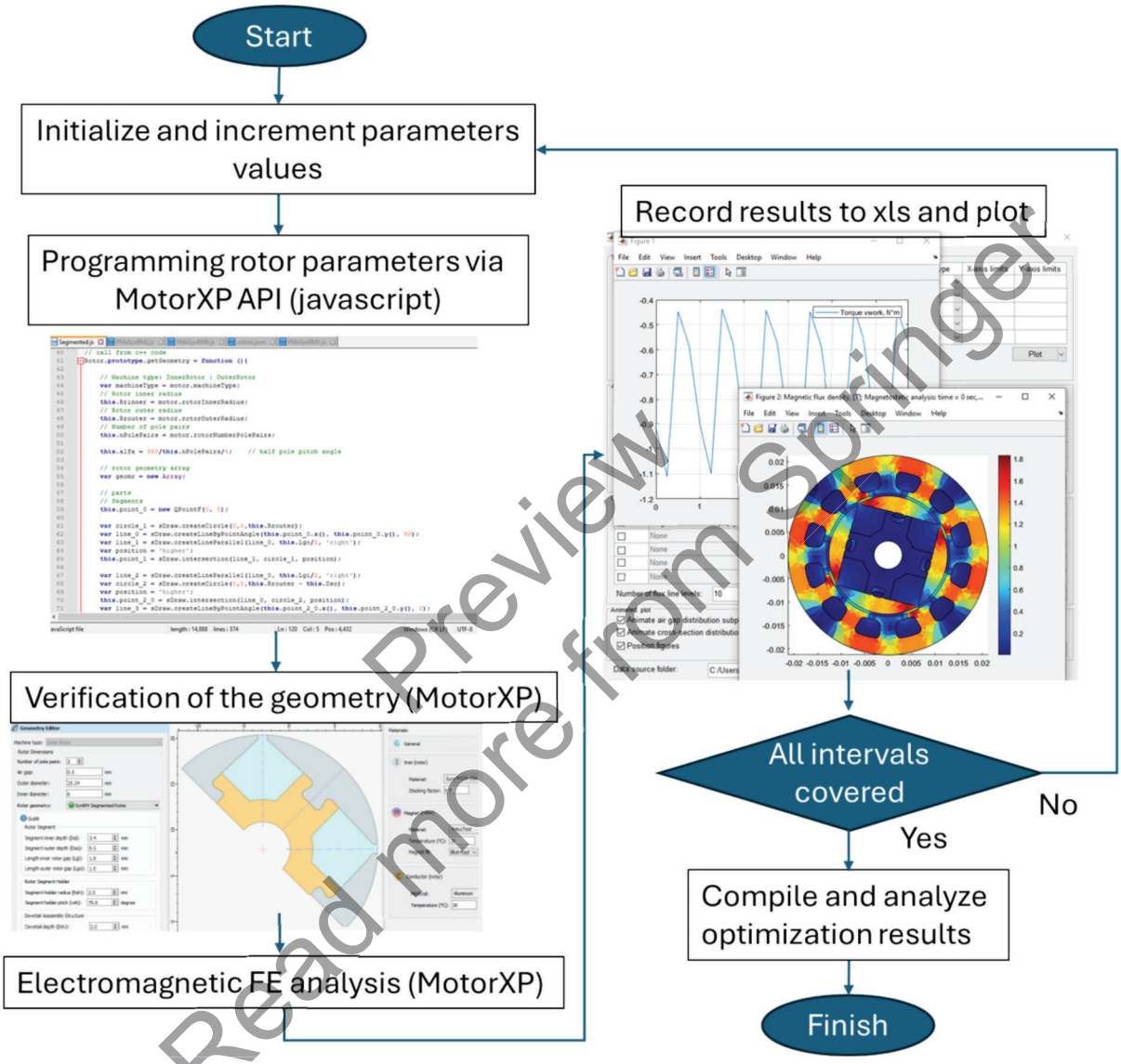

Fig. 7 Flowchart of the rotor parameter optimization process

The optimum dimensions were chosen to construct the final rotor and the magnetic and mechanical analysis are presented in the following section. The complete dimensions of the motor can be found in the Appendix.

2.4 Stator geometry parameters optimization

After identifying the optimal rotor configuration with segment depth d_{seg} = 3.0 mm and rotor pole gap g_{rot} 2.3 mm, we conducted a second optimization phase focused on the stator geometry. This sequential approach allowed us to first determine the most effective rotor topology before refining

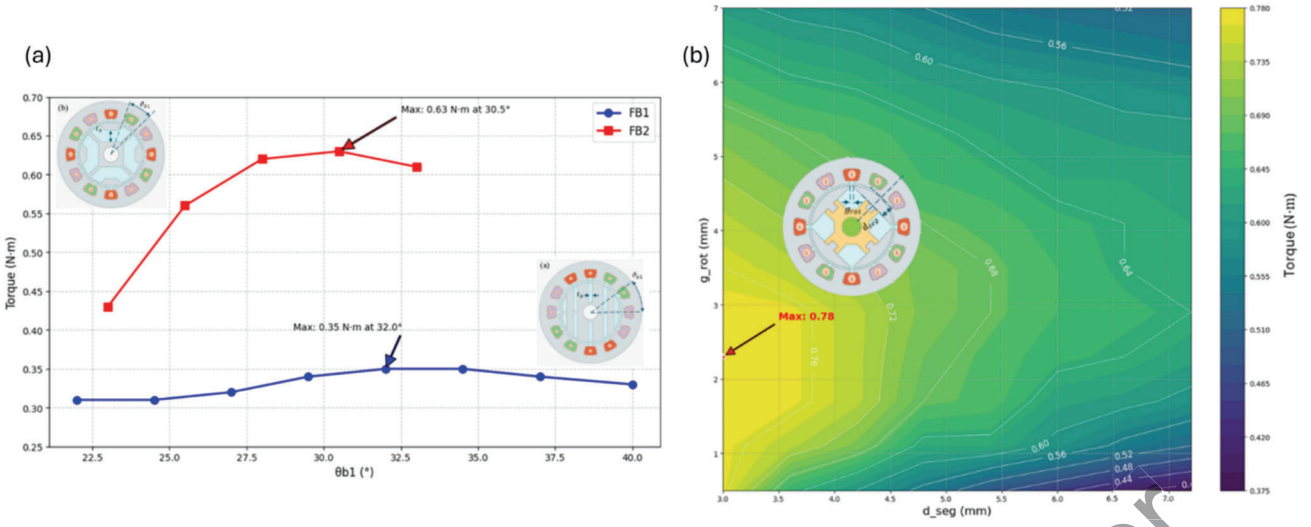

Fig. 8 Torque response to the variation of rotor parameters from the optimization study

the stator design specifically for the segmented configuration. For the stator optimization, we focused on two key parameters that significantly influence electromagnetic performance:

- Stator tooth width (w_t): affecting magnetic loading and core saturation
- Slot opening width (l_{so}): influencing slot leakage flux and effective air gap reluctance, thus torque ripple

These two parameters were selected for optimization based on their critical influence on electromagnetic performance in small-diameter machines. The tooth width (w_t) directly affects the magnetic circuit by determining the cross-sectional area available for flux, thus controlling magnetic saturation levels in the stator. In small-diameter machines, where space is severely constrained, finding the optimal tooth width becomes particularly important—too narrow teeth lead to excessive saturation and reduced performance, while excessively wide teeth reduce slot area and limit the ampere-turns available for torque production.

The slot opening width (l_{so}) was selected due to its significant influence on the effective air gap reluctance and fringing flux. In SynRMs, where the working principle is based on reluctance variation, the slot opening directly impacts the effective reluctance seen by the rotor segments, which affects the torque ripple [30]. Additionally, in small-diameter applications where the ratio of slot opening to air gap is more significant than in larger machines, this parameter has a pronounced effect on performance.

Figure 9 shows that w_t and l_{so} are interdependent. The minimum value l_{so} needs to be at least larger than the airgap to ensure that the flux passes through the airgap into the rotor segment instead of looping in the stator tooth. l_{so} also has a

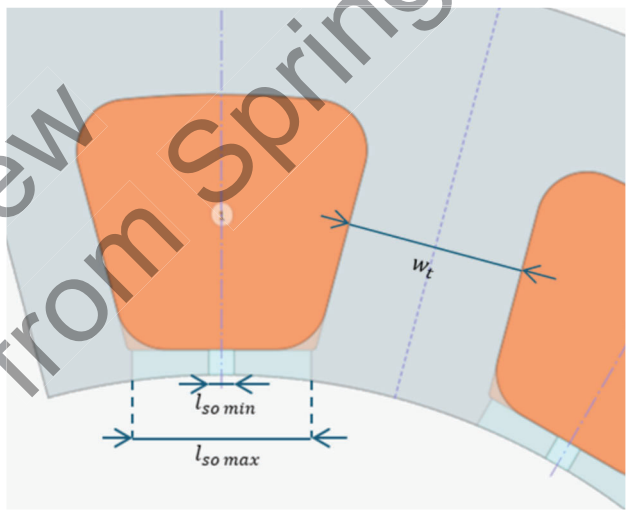

Fig. 9 The two stator parameters to be optimized, w_t and l_{so}

maximum value, which should not exceed the slot width at the opening. It is also noted that l_{so} is inversely proportional to l_{so} and where $l_{so\,\max} = 7.0 - w_t$. Using the Taguchi full factorial DOE approach, all the combinations to be tested are as shown in Table 5 and there are 66 combinations to be tested in total. The result of the optimization is shown in Fig. 10.

The contour plot (left) demonstrates that maximum torque occurs in a region centered around $w_t = 5.5$ mm and $l_{so} = 1.5$ mm, with several parameter combinations (black dots) achieving the peak value of 0.82 N·m. The main effects plot (right) reveals that tooth width exhibits optimal performance within a relatively broad range of 4.0—5.5 mm, while slot opening shows a more pronounced sensitivity with a clear optimum at 1.5 mm. It is interesting to note that our initial

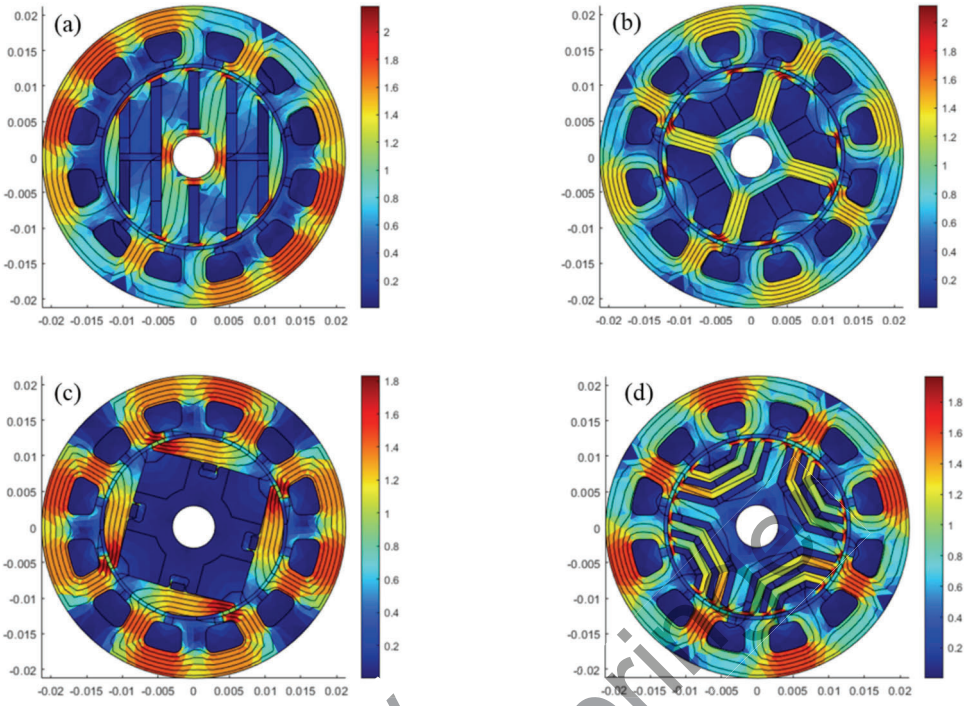

Fig. 12 Flux density distribution at 50A and load angle $\gamma = 45°$. (a) FB1. (b) FB2. (c) Segmented. (d) FB3

Table 7 Torque ripple comparison

Rotor	FB1	FB2	Segmented	FB3
$\Gamma_{avg}(Nm)$	0.34	0.62	0.78	0.97
Torque ripple (%)	51.75	108.13	89.40	13.29

3.2 Torque ripple

Figure 11d presents the harmonic spectrum of the airgap flux density, which directly influences torque ripple characteristics. The FB3 rotor exhibits the highest fundamental harmonic amplitude, followed by the segmented rotor design. All configurations display harmonic components at frequencies corresponding to their pole numbers ($4k$). The FB2 design demonstrates additional harmonic content at frequencies of $2k$, contributing to increased torque ripple. The temporal torque behavior for all four configurations is illustrated in Fig. 13, with their respective average torque (T_{avg}) values and ripple characteristics as summarized in Table 7.

While our geometric optimization focused primarily on maximizing torque output, we recognize that the resulting torque ripple values (89.40% for the segmented design) are significantly higher than desirable for practical applications. Rather than compromising torque density through geometric modifications, we have developed a complementary control-based approach to address torque ripple.

The decision to address torque ripple through control techniques rather than geometric optimization stems from our previous analysis [30] where we identified that the primary

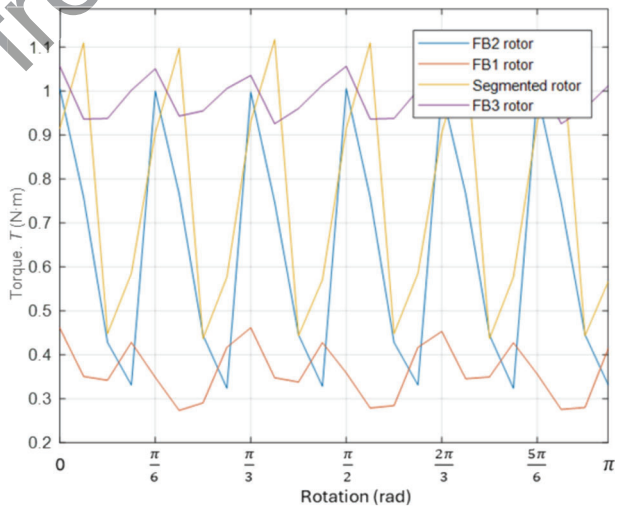

Fig. 13 Torque ripples of the 4 rotors

source of torque ripple in small-diameter segmented SynRMs is the interaction between stator slot openings and the non-magnetic segments of the rotor. These interactions create significant harmonic content in the airgap flux density, particularly at the sixth and 12th orders. In machines with such small dimensions (25.24-mm rotor diameter), attempting to

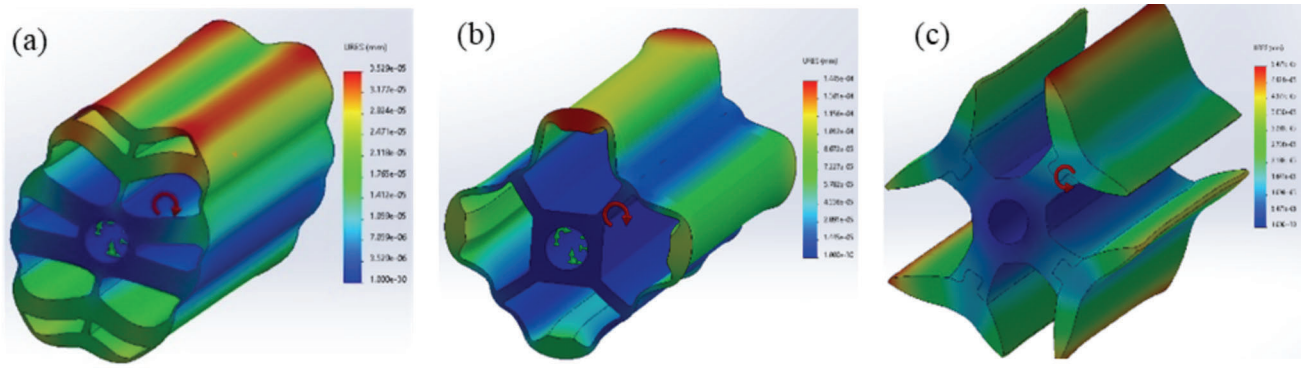

Fig. 15 FE meshing and displacement deformation due to centrifugal force at 5,000 r/min. (a) FB1. (b) FB2. (c) Segmented

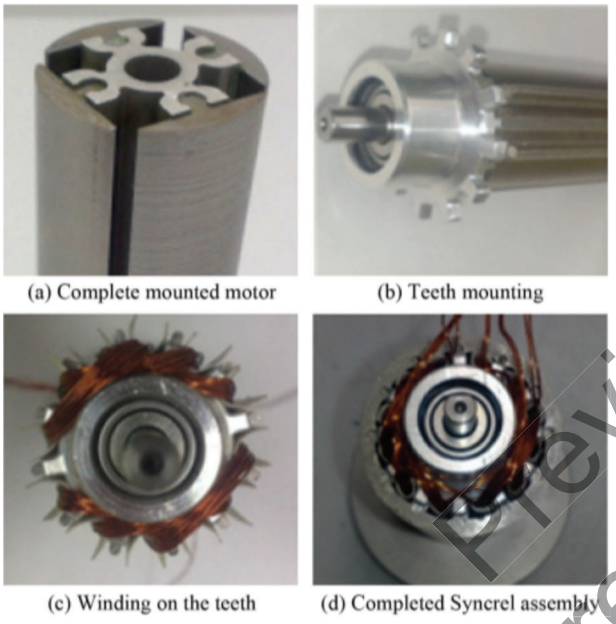

Fig. 16 The segmented rotor SynRM prototype machine assembly details

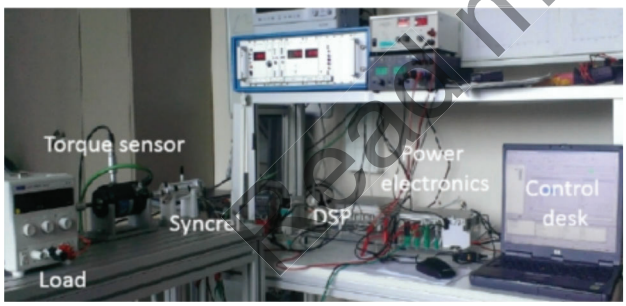

Fig. 17 The complete test bench setup

The speed is measured using a 500 ppr incremental encoder. The torque sensor used is the TG/0.5-BP by Vibrometer with an accuracy of 0.05% out of the full scale of 10 N·m. All the measurements are monitored in real-time via PC host using the Dspace Control Desk. Power delivery is managed by the Rapid Pro power unit, a three-phase PWM inverter using Power MOSFETs, with DC bus limitations of 14 V/30A. The system implements closed-loop speed control following prescribed reference profiles.

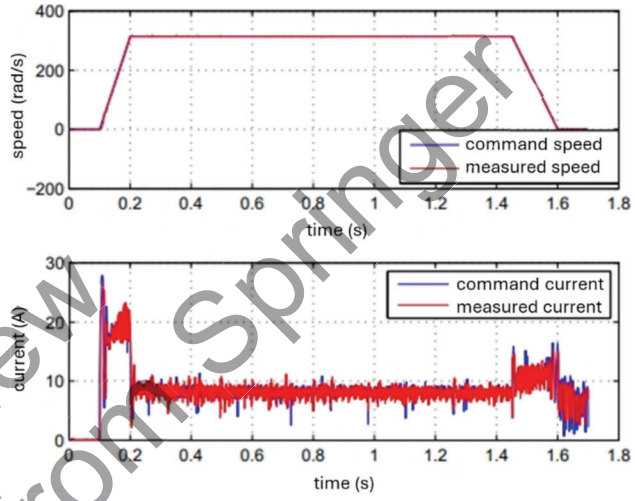

Fig. 18 Speed and current of the SynRM running at a steady-state speed of 3000 r/min

The dynamic performance of the prototype driving a nominal load of 0.15 N·m is illustrated through speed and current responses over time in Fig. 18. The speed profile (upper plot) demonstrates excellent tracking performance, with the measured speed (red) closely following the command speed (blue) during both rapid acceleration and steady-state operation. The machine accelerates from a standstill to 3,000 r/min within 0.1 s, indicating a robust dynamic response. The current profile (lower plot) shows an initial peak of approximately 20A during acceleration, followed by stabilization at approximately 10A during steady-state operation at 3,000 r/min. This behavior reflects typical motor characteristics where a higher current is required during acceleration to overcome inertia, followed by a lower steady-state current to maintain constant speed. The minimal deviation between commanded and measured values in both speed and current responses suggests effective control implementation.